Clustering Approach to Quantify Long Term Spatio-Temporal Interactions in Epileptic Intracranial Electrencephalograph

[1]Anant Hegde, [2]Deniz Erdogmus, [4,8]Deng S. Shiau, [1]Jose C. Principe, [3,4,5,6,7,8]Chris J. Sackellares
[1]Computational NeuroEngineering Laboratory, University of Florida, Gainesville, USA
[2]CSEE Department, Oregon Health & Science University, Portland, USA
Department of [3]Biomedical Engineering, [4]Neuroscience, [5]Neurology, [6]Pediatrics, [7]Psychiatry, University of Florida, Gainesville, U.S.A
[8]Malcolm Randal VA Medical Center, Gainesville, Florida, U.S.A.

***Abstract*—**Dynamical couplings between brain structures are believed to be primarily responsible for the generation of epileptic seizures and their propagation. In this study, we attempt to identify the spatio-temporal interactions of an epileptic brain using a previously proposed non-linear dependency measure. Using a clustering model, we determine the average spatial mappings in an epileptic brain at different stages of a complex partial seizure. Results involving 8 seizures from 2 epileptic patients suggest that there may be a fixed pattern associated with channels's spatio-temporal dynamics during the inter-ictal to pre-post ictal transition.

I. INTRODUCTION

There is sufficient evidence to believe that the brain as a functional model consists of highly complex non-linear dynamics. Application of non-linear dynamical measures [1,2] such as short term Lyapunov exponents (STLmax) and correlation dimension on an epileptic brain has revealed that the complexity of the brain reduces significantly as seizure is approached. In other words, the temporal dynamics of the brain progresses from a 'severe chaotic' state to a much lesser or rather 'mildly chaotic' state.

Much of the analysis on temporal dynamics focuses on analyzing and characterizing the irregular behavior of the time-signal of either intracranial or scalp EEG. However, it is important to realize that the brain is a multi-dimensional system with a large set of neuronal oscillators that are physically coupled together. Obviously the neurons at different spatial locations communicate with each other through synaptic potentials resulting in spike discharges. In such an environment therefore, it would be natural to expect a spatio-temporal interaction at various patho-physiological states. Specifically, in the context of epilepsy, one can perceive that the seizure related abnormal spike discharges and subsequently the seizure events are accompanied by different regions in the brain communicating in a structured fashion. Therefore, it is very essential

to unravel the functional connectivity of the neural networks and analyze how the structures change during seizure events.

Many linear and nonlinear approaches have been developed and even though observations that EEG cannot be distinguished from linearly correlated noise [3] have been made, nonlinear approaches have still been able to extract coupling information in a manner that would not have been possible by spectral approaches. Nonlinear dependencies between multiple signals have been studied in the last two decades, with the hope of enhancing the tool set provided by the linear methods. Unfortunately, they have faced some practical implementation problems as the sensitivity to noise, choice of parameters and the high computational cost. Most of the state-space methods rely on finding the functional dependencies between two time-series based on how their trajectories in the embedded phase space describe each other. Inspired by the similarity–index technique (SI) introduced by Arnhold *et al.* [4], we earlier proposed a self-organizing map (SOM) based computationally efficient measure, SOM-SI [5-6], to measure asymmetric dependencies between time-sequences. Conceptually, the SI and the SOM-SI methods rely on the assumption that if there is a functional dependency between two signals, the neighboring points in the state space of one signal map to the corresponding neighborhoods of its counterpart. The SOM-SI method maps the embedded data from signals onto a quantized output space through a SOM [7, 8] specialized on these signals, and utilizing the activation of SOM neurons to infer about the influence directions between the signals. This approach reduces the computational complexity drastically by exploiting the accurate quantization properties of the SOM in representing the dynamics of the signal in the phase space. Our previous work [6] showed that the SOM-SI was capable of determining the temporal evolution of dependencies between various cortical sites, at different stages of a temporal lobe epileptic seizure.

The epileptic seizures, in particular, are characterized by dynamic states (inter-ictal, ictal, pre-ictal & post-ictal) that are known to possess both local and global spatio-temporal groupings. Channels associate and de-associate in time; however, depending on the psycho physiological state of the brain, certain groups of channels might have a higher likelihood of sharing same channel connectivities, thus forging a long-term association. In epileptic intracranial EEG, identifying such state-dependent clusters may provide us with useful insights on the evolution of brain patterns during seizure states. In this study, we propose a spatio-temporal clustering model to qualitatively analyze the spatio-temporal groupings in multi-dimensional epileptic structures. Unlike in many other clustering approaches where dynamical features extracted from the data are used as basis to determine groupings, our proposed clustering approach uses the dependencies among the original data recordings to do the same. Our approach, in short, essentially seeks to

analyze the regional grouping of cortical sites at different stages of a seizure, based on their mutual interactions.

The paper is organized as follows: We first present a brief review of SOM-SI in section 2. Section 3 discusses the spectral-clustering approach and the proposed spatio-temporal cluster model. Data description is provided in section 4 followed by clinical evaluation of the clustering approach on the epileptic EEG data, in section 5. Section 6. discusses about potential directions for future study.

2. Similarity-Index (SI) Measure

A. Original SI measure

Assume that *X* and *Y* are two time series generated by a system, which are embedded into two vector signals in time using delays. *N(X|Y)* is defined as the average dependency of *X* on *Y* and it can be written as [5],

$$N(X \mid Y) = \frac{1}{N} \sum_{n=0}^{N-1} \frac{R^n(X) - R^n(X \mid Y)}{R^n(X)} \qquad (1)$$

where $R^n(X)$ is the average Euclidean distance between the state-vector of X^n and the remaining state-vectors in X. Y-conditioned Euclidean distance $R^n(X|Y)$ measures the average Euclidean distance between X^n and the vectors in X whose corresponding time-partners are the k-nearest neighbors of Y^n. This measure takes values in [0, 1], where 0 implies no coupling and 1 implies perfect synchronization [4]. Average dependence of Y on X, *N(Y|X)*, is similarly computed. The difficulty with this approach is that at every time instant, we must search for the k nearest neighbors of the current embedded signal vectors among all N sample vectors; this process requires $O(N^2)$ operations. This high complexity hinders real-time implementation and analysis. In addition, the measure depends heavily on the free parameters, namely, the number of nearest neighbors and the neighborhood size ε. The neighborhood size ε needs to be adjusted every time the dynamic range of the windowed data changes.

2.1 SOM-based Similarity Index (SOM-SI)

The Self Organized Map (SOM)-based SI algorithm [5] is fundamentally aimed at reducing the computational complexity of the SI technique. The central idea is to create a statistically quantized representation of the dynamical system using a SOM [7, 8]. A SOM is a neural-network in which spatial patterns from the input-space are mapped onto an ordered output space consisting of a set of neurons, called processing elements (PE). Thus each neuron in the SOM, based on its location on the map, compactly models different features/dynamics of the input.

For best generalization, the map needs to be trained to represent all possible states of the system (or at least with as much variation as possible). As an example, if we were to measure the dependencies between EEG signals recorded from different regions of the brain, it is necessary to create a SOM that represents the dynamics of signals collected from all channels. The SOM can then be used as a prototype to represent any signal recorded from any spatial location on the brain, assuming that the neurons of the SOM have specialized in the dynamics from different regions.

One of the salient features of the SOM is topology preservation; i.e., the neighboring neurons in the feature space correspond to neighboring states in the input data. In the application of SOM modeling to the similarity index concept, the topology preserving quality of the SOM feature of the SOM will be of added advantage, because of the fact that the neighboring neurons in the feature space will now correspond to neighboring states in the input data.

Assume that X and Y are two time series generated by a system, which are embedded into two vector signals in time using delays. Define the activation region of a neuron in the SOM as the set of all input vectors (the embedded signal vectors) for which the neuron is the winner based on some distance metric (Euclidean in most cases). Let X_n be the set of time indices of input vectors x_j that are in the activation region of the winner neuron corresponding to the input vector x_n at time n. Similarly define the set Y_n.

Then the procedure to estimate the directed SOM-SI between X and Y is as follows:

1. Train a SOM using embedded vectors from both X and Y as the input.

2. At time n, find W_n^x, the winner neuron for vector x_n, and find W_n^y, the winner neuron for vector y_n.

3. To find $R^n(X)$, compute the average Euclidean distance between W_n^x and all the other winner neurons in the SOM. Similarly, compute $R^n(Y)$.

4. Determine the sets X_n and Y_n for W_n^x and W_n^y, respectively.

5. Determine the nearest neurons $W_{n,j}^y$ corresponding to vectors y_j, where $j \in X_n$. Determine the nearest neurons $W_{n,j}^x$ corresponding to vectors y_j, where $j \in Y_n$.

6. Calculate $R^n(X \mid Y) = (1/q)\Sigma_{j=1}^q \| W_n^x - W_{n,j}^x \|$, where q is the number of elements in X_n. Calculate $R^n(Y \mid X) = (1/q)\Sigma_{j=1}^q \| W_n^y - W_{n,j}^y \|$, where q is the number of elements of Y_n.

7. Compute the ratios,

$$N^n(X \mid Y) = \left(R^n(X) - R^n(X \mid Y)\right) / R^n(X) \quad (2.1)$$

$$N^n(Y \mid X) = \left(R^n(Y) - R^n(Y \mid X)\right) / R^n(Y) \quad (2.2)$$

8. Find *interdependencies* $N(X \mid Y)$ and $N(Y \mid X)$ as the average of $N^n(X \mid Y)$ and $N^n(Y \mid X)$ over all n.

9. Compute the SOM-SI as the difference,

$$\chi = N(Y \mid X) - N(X \mid Y).$$

Positive values of χ indicate that influence of X on Y is more than the influence of Y on X, while negative values indicate the opposite. Higher magnitude of χ indicates a stronger coupling of the signals.

The computational savings of the SOM approach is an immediate consequence of the quantization of the input (signal) vector space. The nearest neighbor search involves $O(NM)$ operations as opposed to $O(N^2)$ in the original SI, where M is the number of PEs. Traditionally $M << N$, hence, SOM-SI offers a significant reduction in computations compared to original SI.

2.2. Testing the Robustness of SOM-SI on Multiple SOMs

To illustrate the the accuracy of the SOM-based measure, we previously presented a few experimental simulations [5, 9] involving synthetically constructed linear and non-linear interactive models. Results from each of them demonstrated the accuracy of our quantized measure, validated through statistical quantification with results from the original SI measure. For application on seizures especially, a 25 x 25 sized, 2-dimensional SOM grid was trained to embed all the dynamical states of an EEG attractor. SOM being one of the most important elements of this improvised measure, one of the pre-requisites of this approach is to ensure the following: a) that for data modeling purposes, the training set captures the essence of variance found in the dynamics of the ictal states from all the channels, for a given patient and b) the similarity indices computed using the SOM's processing elements (PEs) are independent of the SOM and the corresponding training data set. In other words, pair-wise similarity indices computed on two separate SOMs should be significantly close to each other, if not equal.

While the previous test results [9] were a testimony to the former, the independence of the observed interactions through similarity indices to a given SOM needed to be tested before proceeding with extensive data analysis. From the multivariate EEG data samples of an epileptic patient, two separate training sets were constructed. One of the training sets consisted of portions of data sampled from the inter-ictal, ictal, pre and post-ictal states of seizures 1 & 2 from an

epileptic patient. The other training set consisted of data portions picked around seizure 4 & 5. Using the same normalization procedures on both the sets and with the same set of training parameters as before, two separate SOMs (called as SOM-1 and SOM-2 for convenience) were trained. Following that, the SOM-similarity indices were obtained from pair-wise analysis of interdependence among channels chosen from the ROF and LOF regions of the brain, as illustrated in Fig 1.

The test data from the 3 recording sites in Right Orbito Frontal region (namely ROF1, ROF2 & ROF3) and 3 sites from Left Orbito Frontal regions (namely LOF1, LOF2 & LOF3) were picked from intervals surrounding seizures 4, 5, 6, 7 and seizure 11, respectively. The similarity index profiles $\{N^1 (X|Y)_t$ and $\{N^2 (X|Y)_t$ obtained from computing the SOM-SI on large intervals (say time t = 1,…,T) of seizure data are quantitatively compared using the classical correlation coefficient and error-percentage as the comparison metrics. The error-percentage is computed as follows:

$$\{e\} = 100 * \left\{ \frac{N^1(X \mid Y)_t - N^2(X \mid Y)_t}{N^1(X \mid Y)_t} \right\}_{t=1}^{T} \tag{3}$$

where N(X|Y) is the normalized interdependency of X on Y. Note that the notations X are Y are used to denote the two channels of interest. Normalized error *e* quantifies the percentage difference between the interdependency values from SOM-2 and SOM-1, keeping interdependency value from SOM-1 as the reference. From the error population, the fraction of the absolute error values less than 20% and the fraction less than 10% are computed to determine the degree of dependence of the SOM-SI measure on the data used to train a SOM.

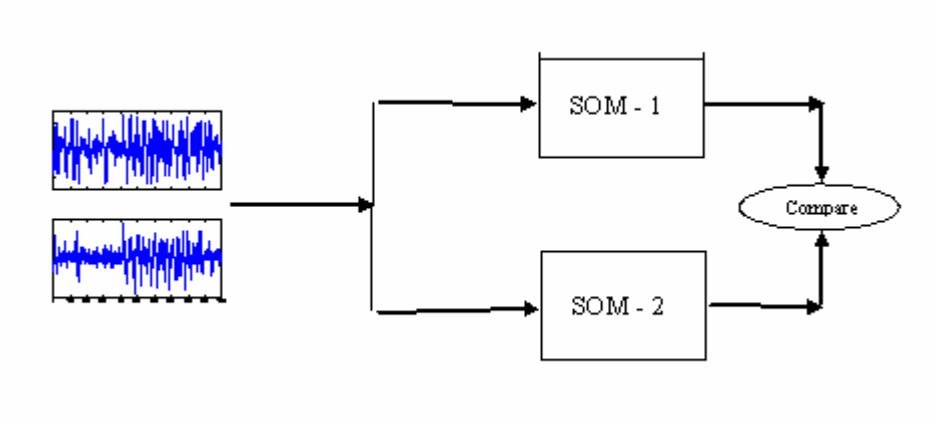

Figure 1. Experiment setup to compare SOM-Similarity Indices obtained from 2 separate maps.

For illustration, the results from analyzing the interdependency of LOF3 on LOF4 on various seizures are shown in fig 2. The histograms correspond to the error ensembles obtained from

analyzing over long seizure intervals. Qualitatively, the superimposed traces in fig 2 indicate the extent of agreement or disagreement between the SOM-SI profiles. Table 1 compiles a summary of the agreement between the SOM-SI profiles for about 13 hours of EEG data. A large fraction of errors less than 20%, supported by a high correlation coefficient between the two SOM-SI profiles suggests that there was very little disparity between the SOM-SI profiles from SOM-1 and SOM-2. Besides, the high percentages also suggest the EEG data dynamics do not vary drastically from one seizure to another, and therefore the two SOM models produced the almost identical SI results. This finding will consequently support (or reinforce) our original belief that a well-trained SOM and a well picked training data set is sufficient to carry out inter-dependency analysis on all the seizures of a patient.

Overall, pair-wise analyses of the interdependency among 6 channels (C_2^6 = 15 combinations) on 5 seizures of the epileptic patient was performed on SOM-1 and SOM-2. The average correlation coefficient and the error results between the SOM-SI profiles are shown in Table 2.

Results from table 2 indicate that around 80% of the times, the differences between the SOM-SI results are less than 20%. This is not surprising considering that the differences are measured in percentages (3) and therefore even small discrepancies in the case of small dependency values can appear magnified. In addition, we also speculate that the discrepancies could be the outcome of the two SOMs being trained in an identical fashion instead of being fine-tuned to obtain the lowest reconstruction error in each. In

Table 1. Quantitative comparisons between the SOM-SI profiles obtained from SOM-1 and SOM-2. LOF3 & LOF4 data was projected on each of the SOMs and then the SOM-SI measure was applied to analyze the dependency of LOF3 on LOF4.

Interdependency N(LOF3| LOF4)	**Correlation Coefficient (%)**	**Fraction of error less than 20%**	**Fraction of error less than 10%**
Seizure 6 & 7	95.74	0.8504	0.5597
Seizure 4 & 5	98.45	0.9234	0.7543
Seizure 11	91.59	0.6452	0.3614

general, if the SOMs can be designed to obtain the lowest reconstruction error, by iteratively choosing the best sets of parameters, a slight improvement in the performances can be easily achieved. But as it stands, a slight discrepancy can nevertheless be always expected although it may have very little impact in the overall scheme of analysis.

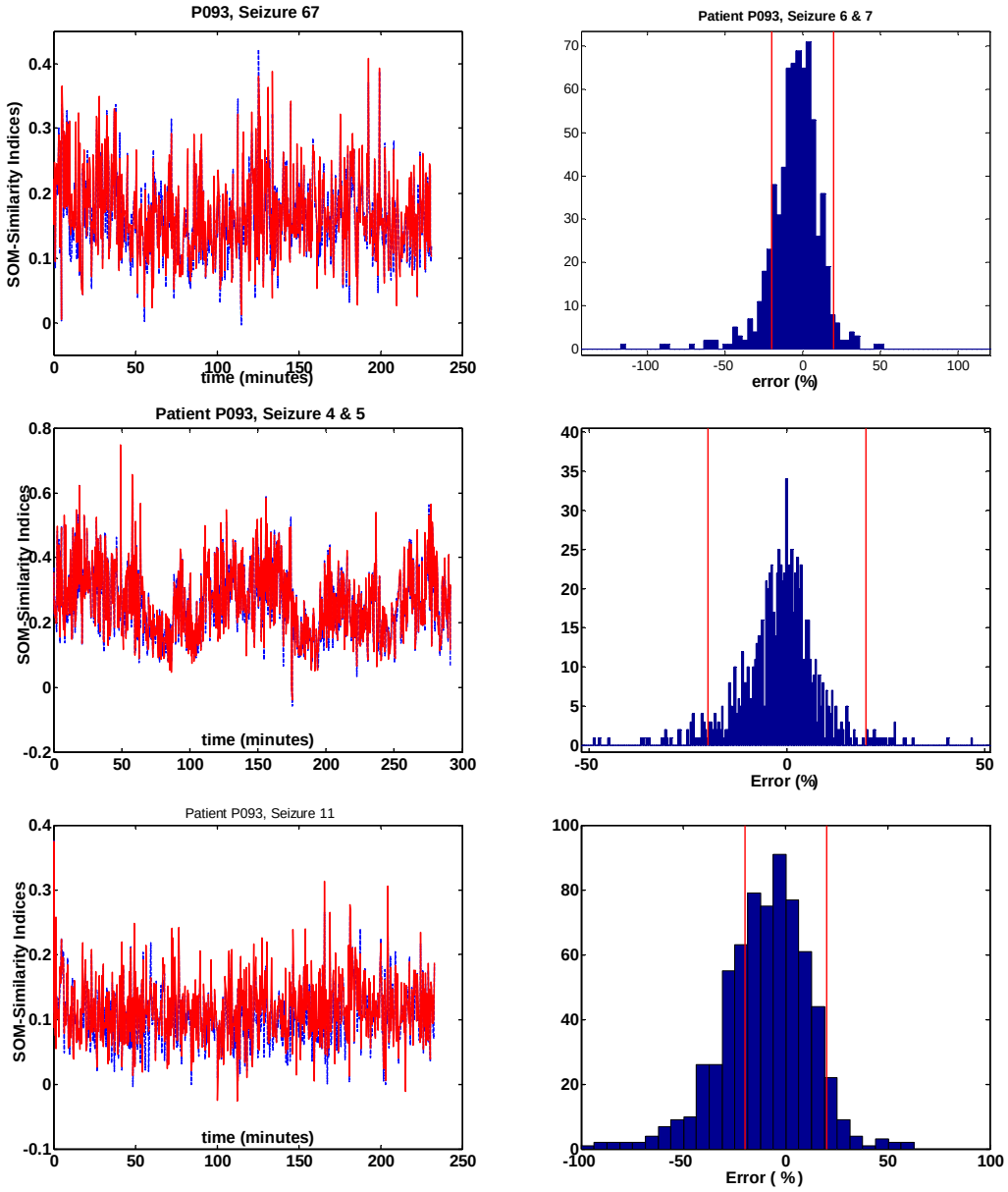

Figure 2. Comparing interdependencies between channels LOF3 and LOF4. Left : SOM-similarity profiles from the output of SOM-1 and SOM-2 are superimposed. Right: Histogram of the errors in %. Top: Seizure 4 & 5 Middle: Seizure 6 & 7. Bottom: Seizure 11.

Table 2. Summary of the comparisons between the SOM-SI profiles from SOM-1 and SOM-2. Each row represents the statistics (mean and variance) of pair-wise SOM-SI analyses of the epileptic EEG data from 6 channels (15 combinations).

	Correlation Coefficient (%)	Fraction of error less than 20%	Fraction of error less than 10%
Seizure 6 & 7	94.32 ± 2.85	0.79± 0.1	0.54 ± 0.12
Seizure 4 & 5	97.46 ± 1.08	0.91 ± 0.06	0.73 ± 0.12
Seizure 11	93.24 ± 2.06	0.71 ± 0.08	0.41 ± 0.07

3. Spatio-Temporal Clustering Model

In the previous section, we provided a brief description on the SOM-SI measure and demonstrated SOM's resourcefulness as a model infrastructure for computational purposes. Often, the time-sequences in a multi-variate system share similar information that is reflected in their interactive or synchronization abilities. By definition the word similar could mean that the information shared among a set of channels is stronger than the information they share with other channels. Such spatial similarities could possibly be momentary up to a few seconds or could even stretch to several minutes or hours. As we postulated earlier, dynamial similarities in spatio-temporal behavior could be one of the driving factors to trigger certain events in biological systems. From a seizure point of view, we believe that analyzing the temporal changes in channel similarities could reveal some interesting aspects about the epileptic brain.

Similarity-based time-series clustering [10, 11] is a well researched topic in the area of dynamical graph theory. It is an extremely useful approach to characterize the spatial groupings in time-sequences. Similar time sequences are typically grouped based on their mutual interactions. In this study, using the SOM-SI as a computational tool to derive the distance/similarity/proximity matrix, we propose a clustering model to dynamically analyze the spatio-temporal groupings in muti-variate time sequences.

3.1 Model for Spatio-Temporal clustering

In this section, we propose a clustering approach to extract information on spatio-temporal distribution of multivariate time-measurements. A 3-fold approach consisting of spatial-discretization of the data using spectral-clustering technique [12, 13], temporal quantification using hamming distance, followed by application of another clustering technique, is presented in Fig 3. The rational will become apparent during the explanation.

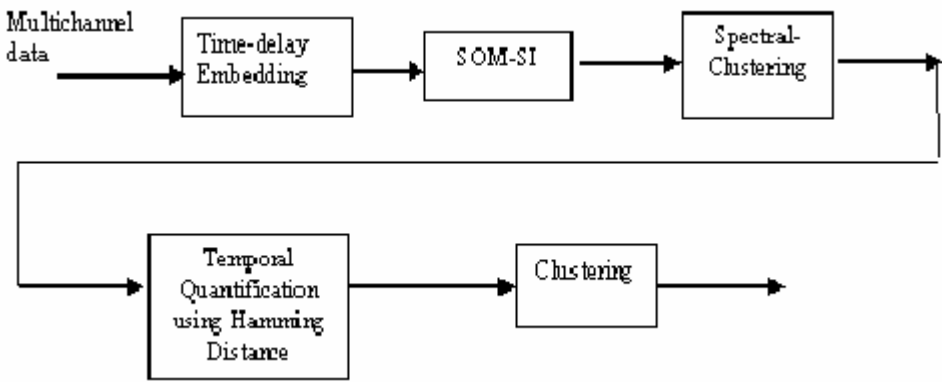

Figure 3. Block diagram to extract spatio-temporal groupings information in Multivariate EEG structures

Spectral clustering is one of the many clustering methods that use subspace decomposition on data-derived affinity matrix to achieve data-clustering. Using kernel methods, the data samples are projected onto a higher dimensional space where the discriminant analysis is much easier. Projecting the data onto a feature space results in tightly formed clusters such that the between cluster entropy is maximized and within cluster entropy is minimized. In our study, we use the standard spectral clustering algorithm by Ng *et al*. [13] to spatially cluster the similarity-indices obtained by the SOM-SI technique.

Pair-wise evaluation of SOM-SI measure on all the possible combinations (($C^N_{2,}$ where N is assumed to be the number of channels) of a portion of a multi-variate time series leads to $k = 2*(C^N_2)$ similarity indices in the bounds of [0, 1]. k is multiplied by 2 because of the asymmetric nature of the SOM-SI measure. If we imagine the time-series as various inter-connected nodes in a multi-dimensional graph, the SOM-SI similarity indices represent the affinity or rather, the weights of the connection, between those nodes. Therefore, we can translate them into a square matrix of size N x N, where N is the # of channels. Since the weighting is normalized between 0 and 1, the diagonal elements representing the affinity of a channel with itself, are coded as 1.

However, to be able to perform spectral-decomposition on an affinity matrix, Ng's algorithm [13] requires that the affinity matrix be square and symmetric in nature. This is because

the eigen decomposition yields orthogonal column vectors (also called eigenvectors) only if the projection matrix is square-symmetric. The asymmetric matrix can be transformed to a symmetric matrix by adding it to its transpose and dividing each entry by 2. Following the eigen decomposition on the transformed affinity matrix, we have a set of labeled clusters representing the membership of the channels.

If the above procedure is repeated over consecutive time windows (overlapped or non-overlapped), channel groupings obtained on each time-window can be arranged as in a matrix form as in (4).

$$\kappa_{spect} = \begin{bmatrix} 3 & 2 & 2 & . & . & . & . & . & 3 & 1 \\ 1 & 2 & 2 & . & . & . & . & . & 3 & 2 \\ . & . & . & . & . & . & . & . & . & . \\ . & . & . & . & . & . & . & . & . & . \\ 3 & 1 & 2 & . & . & . & . & . & 1 & 2 \end{bmatrix} \quad (4)$$

To characterize the average clustering of the channels over a longer period of time, we propose another, albeit simple, hierarchical clustering approach that uses hamming distance to derive the proximity matrix.

3.2 Temporal Quantification Using Hamming Distance

We showed in the previous section that the multivariate time-series can be grouped by using similarity-based clustering techniques such as spectral clustering. The spectrally clustered labels specify the groups of channels exhibiting high degree of within-cluster similarities and low between-cluster similarities. Often in applications such as epileptic EEG analyses where associations last longer, it is important to identify channel groupings over a longer time-window.

State dependent connections can be quantified by clustering rows of the κ_{spect} matrix that are similar with each other over a longer time interval, say *T*. In this context, we propose a simple statistic that computes the relative frequency of any two channels sharing the same labels/groupings to determine the degree of similarity. In other words, in a time window of length *T*, we check the average number of times when the two channels of interest, share the same cluster label.

In an algebraic context, the above operation is equivalent to computing pair-wise hamming distance in a time window *T*. Similarity can be quantified by subtracting the hamming distance from 1. That is,

If d_{ij}^{ham} is the hamming-distance between channels ‘i’ & ‘j’, similarity in probabilistic terms can be obtained as,

$$p_{ij}^{sim} = 1 - d_{ij}^{ham} \quad (5)$$

Thus, computing the pair-wise similarity for all *i* & *j* combinations will result in a ***P*** matrix of size *N x N* (*N* is the number of channels). For convenience, we will call the matrix ***P*** the cluster-similarity matrix in all our future references.

Hierarchical clustering on the cluster-similarity matrix ***P*** will yield information on the cluster groupings over a time *T*. In the context of EEG data, clustering will thus enable us to know the groups of channels that have similar behavioral structure in the brain, over a longer time frame.

4. Epileptic EEG Data Description

Intracranial EEG signals were recorded from hippocampus, sub-temporal and frontal-cortex structures of epileptic patients having a history of complex-partial and partial-secondary seizures of temporal-lobe focus, using bilaterally and surgically implanted electrodes (Fig 4). Using amplifiers with an input range of $\pm 0.6\boldsymbol{mv}$, the recorded signals were converted to narrow-band using an anti-aliasing filter with a cut-off range between 0.1Hz and 70Hz. Using an analog-to-digital converter with 10-bit quantization precision, the narrow-band signals were sampled/digitized at 200 samples/sec. Measurements involved recording EEGs from multiple sensors (28 to 32, with common reference channels) and the recordings spanned over 6 continuous days. A total of 55 seizures, of temporal lobe onset, were recorded from 5 patients, in the range of 6 to 18 seizures for each patient.

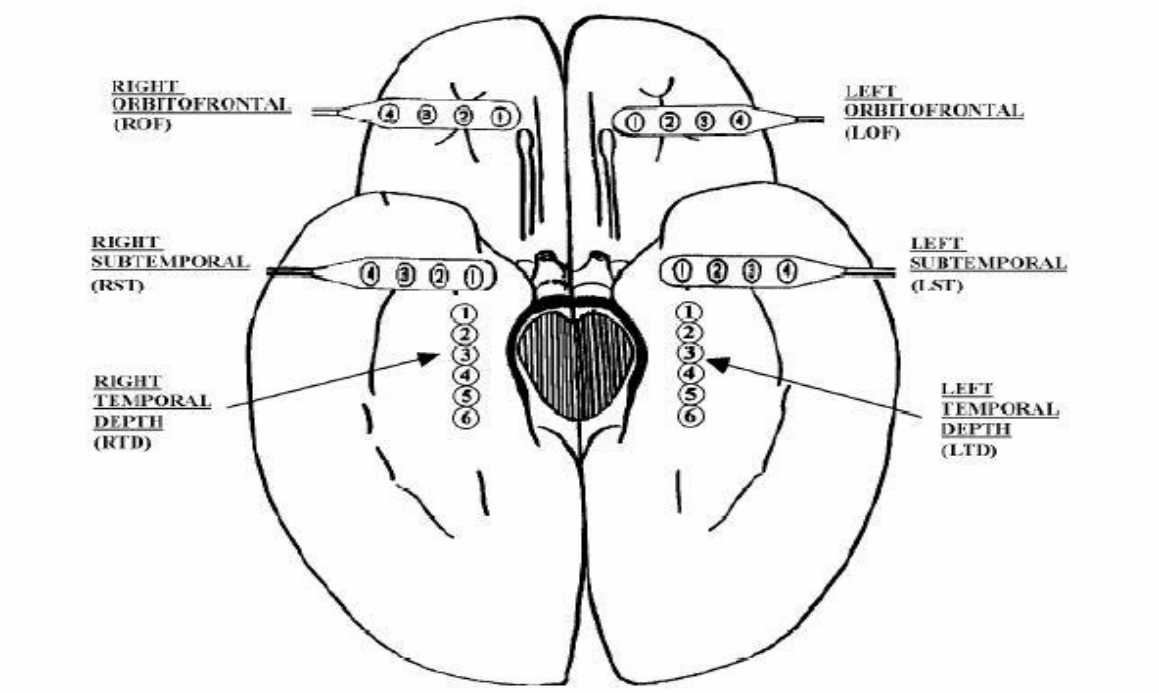

Figure 4. Diagram of the depth and subdural electrode montage in an epileptic brain. Electrode strips are placed over the left orbitofrontal (LOF), right orbitofrontal (ROF), left subtemporal (LST), right subtemporal cortex (RST). Depth electrodes are placed on the left temporal depth (LTD) and right temporal depth (RTD), to record hippocampus EEG activity.

5. Results

In the last section, we proposed a spatio-temporal model to extract groupings from long term multivariate recordings. In this section, we will focus on the application of that model on the epileptic intracranial EEG time series. The first part of the section will describe the details on the application of the model and the second part will discuss the results of analyses on 8 seizures, from 2 patients.

5.2 Application on Epileptic Intracranial EEG Data

The temporal changes in the spatial structure of an epileptic brain was analyzed on twenty four (24) representative channels recorded bilaterally from the orbito-frontal, temporal and sub-temporal regions on the brain. One of the fundamental requirements for analyzing the dynamics of a non linear system is to construct the state-space attractor from just a single recording of the time-series. From previous studies that estimated intracranial EEG attractor size using correlation-dimension techniques [14, 15], we know that the EEG state space is bounded between 3 and 10. This is of course assuming that the data is entirely noise-free and infinite amount of measurement data is available. The large range in dimension is due to the fact that the properties

of the EEG dynamical system undergo dimension changes with changes in brain's physiological states and pathological conditions. On our intracranial EEG data, the embedding dimension (m) and the delay(τ), however, were chosen to be m = 10 and τ = 4. The parameters were compatible with other studies [14, 15], performed on the same data.

The following steps describe the procedure to track the spatio-temporal connectivity patterns in intracranial EEG data.

1. Choosing suitable embedding parameters, intracranial EEG attractors in higher dimensional state space is constructed using Taken's time-delay embedding theorem [16]. On 10 second epochs, pair-wise analyses of interdependence among 24 channels are computed using the SOM-SI measure.

2. The similarity indices, from every window, are translated into a symmetric similarity/affinity/proximity matrix. With the number of clusters (say n_1) specified apriori, spectral clustering on the affinity matrix results in channels being labeled as one of the n_1 clusters.

3. Steps 1 to 3 are repeated for all the successive windows, representing 10-second stationary segments. However, the overall ability of the channels to associate with each other over a longer time-duration needs to be quantified.

On 30 minute time segments (equal to 90, 10-second windows), pair-wise Hamming-distance based cluster-similarity matrix *P* is computed among all the channels. The matrix elements essentially index the probability of channels to group into the same cluster over a 30 minute time interval.

Spectral clustering or any other clustering algorithm on the cluster-similarity matrix *P* will result in final cluster memberships. The number of clusters is fixed to n_2.For computing similarity indices in step 1, the epoch length of 10 seconds is chosen as a tradeoff between stationarity and sample-size requirements. Also note that the successive windows are 10 seconds apart (alternate 10 second windows), for reasons specific to computational feasibility.

We now describe step 2, with more details. The channel interdependencies obtained from SOM-SI represent the spatio-temporal correlation indices obtained by computing pair wise similarity-index among 24 channels. In spectral clustering jargon, the resulting matrix can be interpreted as an affinity matrix representing the pair-wise distances between 24 nodes. After spectral-clustering, we have a set of labeled clusters representing the membership of the channels

[17]. Repeating this procedure on every 10-sec window will yield a discrete-valued matrix κ_{spect} similar to (4).

Typically, the choice for the number of clusters n_1 in step 3 is conditioned on the significant eigen-values (say 90 %). In our analysis, the sum of first 3 eigen-values typically ranged from 60% to 80% of the total variance, due to changes in seizure states. Considering this variability between epochs and the fact that the number of clusters need to be the same for all epochs in order to be able to determine the overall grouping in channels (using cluster-similarity matrix *P*), we fixed the membership size to $n_1 = 3$.

The notion of pre-seizure state has widely been debated upon. A lot of studies argue against the notion of a 'pre-seizure' state transition. However, experimental studies using non linear dynamics have shown that the quantitative descriptors of EEG exhibit seizure pre-cursors in the form of inter-ictal to pre-ictal state transitions. The pre-ictal transition time is not exactly known, however literature suggests that it has a broad range of 5 minutes to 120 minutes before seizure. Therefore in step 5, as a tradeoff between state transition periods and time-resolution, we choose 30 minutes time window to characterize both the pre-ictal and the post-ictal periods.

Following are the clustering results from applying the spatial-clustering procedure on different seizures.

Patient P093

This patient had a history of complex partial seizures, localized in the mesial structures of the temporal lobe. Surgery revealed a lesion in the right hippocampus (RTD electrodes) region.

The set of 24 channels are listed below,

Channels 1 to 4: {LTD3, LTD5, LTD7, LTD9}

Channels 5 to 8: {RTD4, RTD6, RTD8, RTD10}

Channels 9 to 12: {LST1, LST2, LST3, LST4}

Channels 13 to 16: {RST1, RST2, RST3, RST4}

Channels 17 to 20: {LOF1, LOF2, LOF3, LOF4}

Channels 21 to 24: {ROF1, ROF2, ROF3, ROF4}

Before data analysis, a validation test was performed to check whether application of different clustering algorithms on ***P*** would consistently result in same cluster memberships or not. For a given number of clusters n_2, it turned out that all the clustering algorithms including spectral clustering produced the same outputs. Therefore, we decided to choose the simple hierarchical clustering algorithm used in the Matlab 6.5 package owing to its graphical support.

Cluster-similarity matrices ***P*** indicating the probability that two channels share the same grouping in a 30-minute time segment are shown gray-scale coded in Fig. 5. Pre-seizure analysis

on 30-minute windows is shown for up to 3 hours. Similarly, the post-seizure analysis is shown for the first 30 minutes. The ability of the left side channels to have a higher tendency to group together compared to the right hemisphere channels is quite noticeable from fig 5. In addition, the orbito frontal lobes seem like the only area on the brain to have a high probability of making a cross-hemisphere grouping. On the left hemisphere, the LST and the LTD channels are consistently seen to share the same clusters.

To confirm the observations from fig 5, the hierarchical clustering algorithm was applied on each of those ***P*** matrices. Fig. 6 graphically illustrates two instances of the clustering outputs through dendrograms. A dendrogram is strictly defined as a binary tree with a distinguished root that has all the data items at its leaves. Conventionally, all the leaves are shown at the same level of the drawing. The ordering of the leaves is arbitrary. The heights of the internal nodes are related to the metric information (***P*** here) used to form the clustering. Using a threshold of 0.4 and the average-linkage technique to determine fusion levels, clustering was performed on a pre-defined number of clusters (n_2). For determining apriori the number of clusters n_2, several dendrograms were visually analyzed. There seemed to be at least 3 to 4 strong groupings among channels in most of the dendrograms. For consistency, therefore, we chose to fix the number of clusters *n2* to 3 for all the analyses.

Both dendrograms in fig 6. clearly translate the spatial patterns observed in the corresponding ***P*** matrices of fig 5. The top dendrogram in fig 6. corresponds to the 2.5 hours to 3 hours time window (indicated by -5) in fig 5. It is easy to see that the dendrogram considers the RTD and the RST as isolated clusters due to their weak between-cluster fusion level. Since the number of clusters n2 is restricted to 3, all the remaining channels form a single large cluster. Similarly, the bottom dendrogram in fig 6. corresponds to the P matrix indicated by -1 in fig 5. In this case, the RST and the RTD channels group into one cluster; also well supported by a dark patch in fig 5. This enables the LST/LTD channels and the LOF/ROF channels to group together as separate clusters.

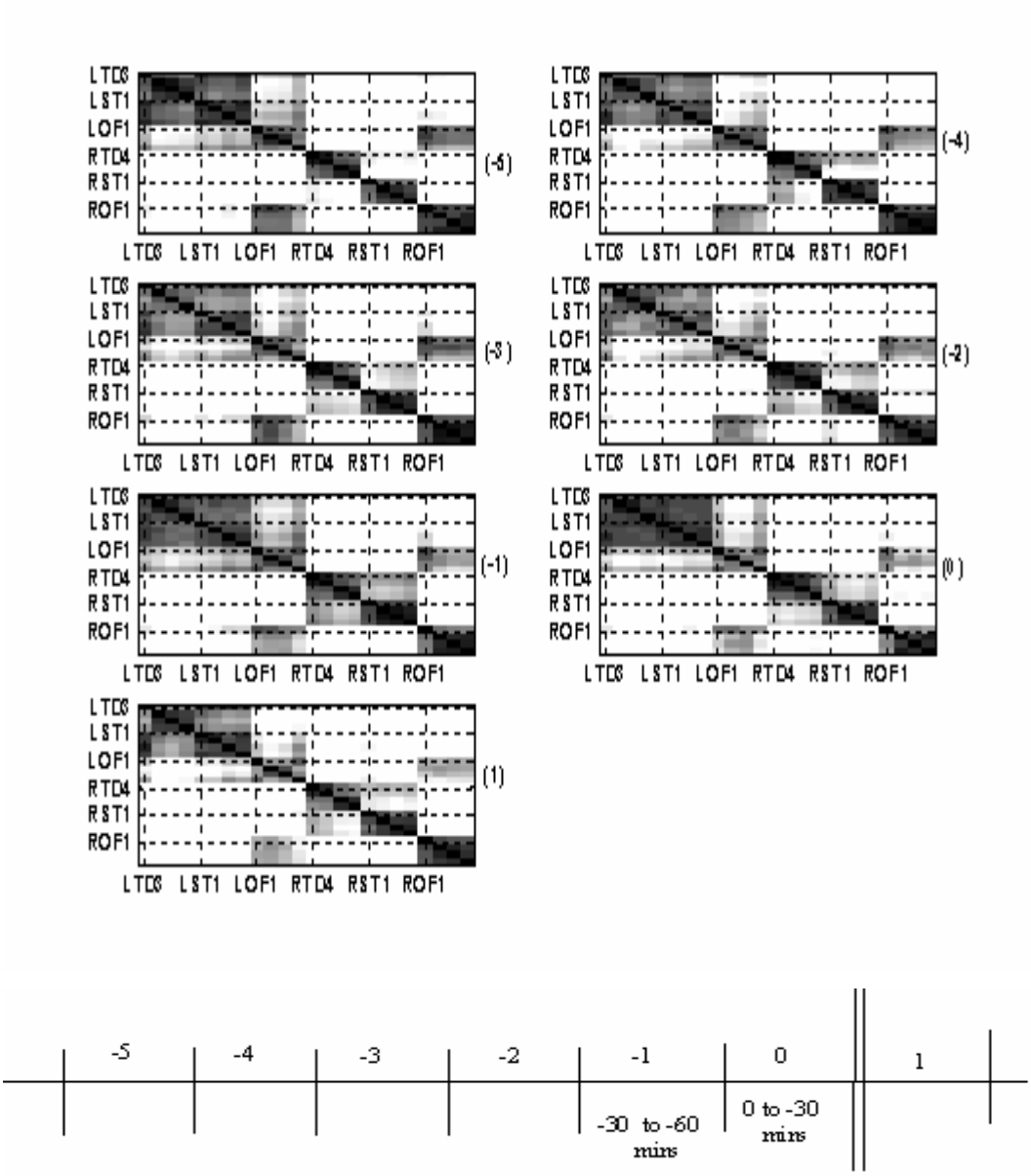

Figure 5. Seizure 11 of patient P093: Cluster-similarity matrices P indicating the probability that two channels share the same cluster label in a 30 minute time-interval.

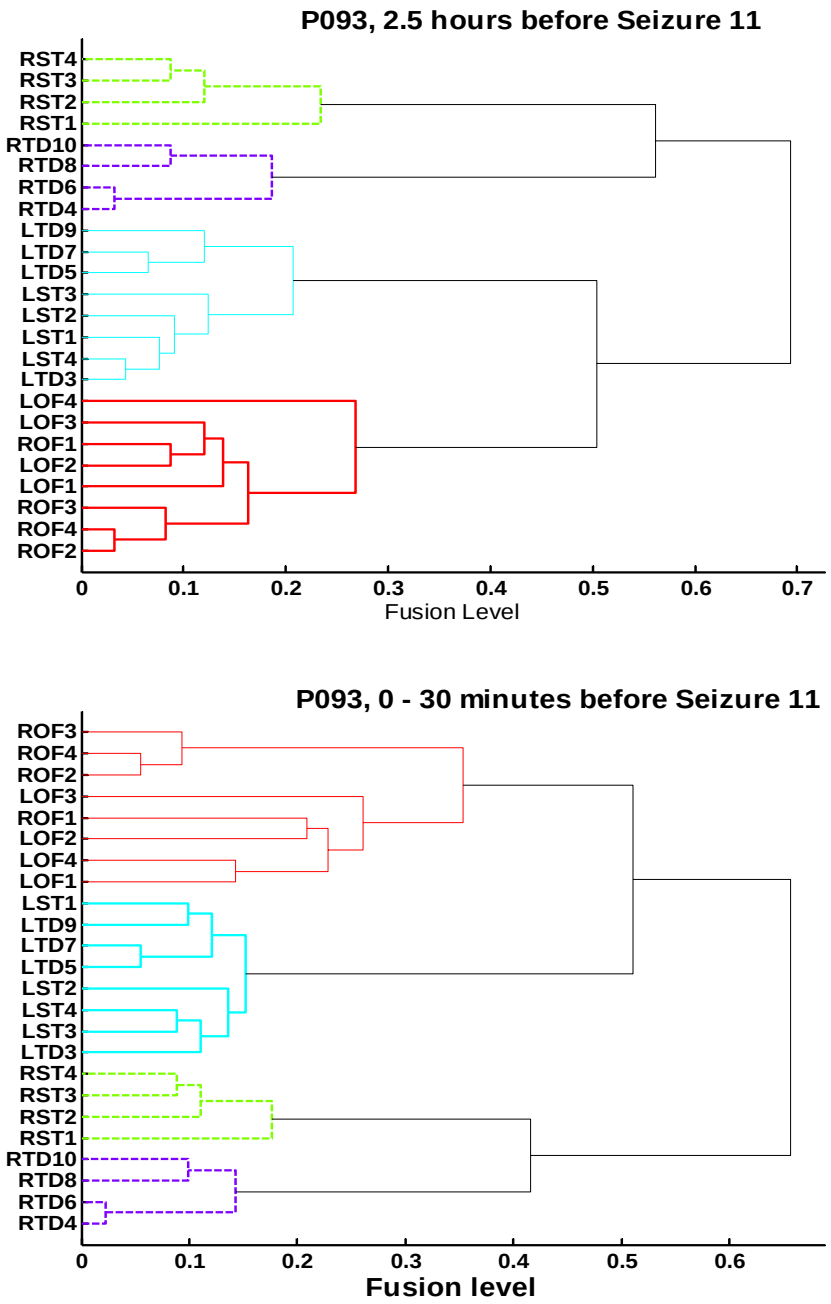

Figure 6. Dendrogram representation of the cluster results in Seizure 11, P093. TOP: Dendrogram corresponding to 2.5 hours before seizure. BOTTOM: Dendrogram corresponding to the 30 minute pre-seizure period.

The overall cluster configuration is listed in table 3.

Table 3. Spatio-temporal groupings as obtained for seizure 11 of patient P093

P093, Seizure 11	**C_1**	**C_2**	**C_3**
Pre seizure, (2.5 – 3 hrs)	RTD	RST	LTD, LST, LOF, ROF

Pre seizure, (2 – 2.5 hrs)	RTD, RST	LOF, ROF	LTD, LST
Pre seizure, (1.5 – 2 hrs)	RTD, RST	LOF, ROF	LTD, LST
Pre seizure, (1 – 1.5 hrs)	RTD, RST	LOF, ROF	LTD, LST
Pre seizure, (30mins – 1 hr)	RTD, RST	LOF, ROF	LTD, LST
Pre seizure, (0 - 30mins)	RTD, RST	LOF, ROF	LTD, LST
Post seizure, (30mins – 1hr)	RTD, RST	LOF, ROF	LTD, LST

We summarize the spatial patterns at different time-intervals of seizure 11 as follows:

1. The LST and the LTD channels in particular, exhibit a strong tendency to belong to the same group.

2. The LOF and the ROF channels form a strong bi-lateral homologous connection, as seen from all the matrices in fig 5.

3. Relatively strong similarity can be seen between RTD and the RST channels.

4. Common observation in all the matrices is the strong similarity between the left hemisphere channels as opposed to the right hemisphere channels. This is reflected in the ability of LOF channels to have a higher probability of sharing clusters with other left-hemisphere channels, as seen in Fig 5.

5. Interestingly, no temporal changes are seen in the spatial-patterns yet.

5.3 Statistical Validation

The cluster configurations observed from analyzing 30 minute segments necessitates validation. Previously [9], we partially validated our model (until the spectral clustering stage), using synthetically coupled multivariate time sequences (non linear and linear, both). Simulations involving creation of dynamic graphs involve multidimensional time series that continuously change cluster memberships over time. Determining the average spatio-temporal groupings from a collection of multi-variate time-series is relatively easier to demonstrate in linear coupling cases. However, non linear dynamic model constructions are extremely hard and mostly, non-trivial. We therefore decided to pursue a posterior verification of the time-averaged cluster groupings on the intracranial EEG data, using the quasi-surrogate analysis [18-20], technique.
Recall that the cluster groupings obtained over 30 minute time-segments involve two steps. First step consists of applying spectral clustering technique on the SOM-similarity indices (computed on 10 second intracranial EEG data segments). Then similar grouping patterns among channels

are extracted by using hierarchical clustering approach on the cluster-similarity matrices ***P***. In order to validate this 2-step approach, we define our hypothesis as follows

H_0: The average within-cluster channel interaction at each window (out of 91 10-second windows) is not significantly different from the corresponding between-cluster channel interactions.

We propose to test this hypothesis on all the 3 (n_2) clusters separately, for every 10-second window within the 30 minute period.

Within-cluster interaction is computed by averaging the pair-wise similarity indices for all the channels within a cluster. For between-cluster interaction, the pair-wise interactions between 3 channels, picked randomly from each of the 3 clusters are computed. A between-cluster interaction statistic is formed by computing the average interactions from random selection of 3 channels (one from each cluster), over a number of trials. We found that this statistic follows a quasi-normal distribution, implying that the within-cluster interaction value can now be compared with the mean and the variance sample estimates of the between-cluster statistic. Mathematically, we construct the z-score as follows

$$Z_t^i = \frac{\left| C_{w_t}^i - \left\langle C_{b_t} \right\rangle \right|}{\sigma(C_{bt})} \quad \text{t = 1, 2,.. ,90 \& i = 1, 2, 3.} \tag{6}$$

where C_{wt}^i is the within-cluster interaction at time '*t*', for cluster '*i*'. $\left\langle C_{b_t} \right\rangle$ is the mean and $\sigma(C_{bt})$ is the standard-deviation of the between-cluster interaction at time '*t*'. Z_t^i reflects the z-score and is considered significant at the 95 percentile significance if $Z_t^i > 1.96$ (reject H_0). In table 5 the bolded value in each cell represents the number of windows (out of 91) having significant z-scores in the 30 minute period corresponding to fig 5 (P093, Seizure 11). It is easy to observe that the null-hypothesis H0 is rejected beyond doubt, validating the clustering results.

Table 4. P093, Seizure 11: Over each 30 minute (91 samples total) window, number of times the within-cluster interaction is greater than between-cluster interaction, at 95% significance level.

P093, Sz 11	**-5**	**-4**	**-3**	**-2**	**-1**	**0 (Sz)**	**1**
C1	1	1	0.91	0.95	0.99	1	0.93
C2	0.82	0.89	0.96	0.91	0.89	0.85	0.98
C3	0.95	0.55	0.80	0.70	0.46	0.46	0.97

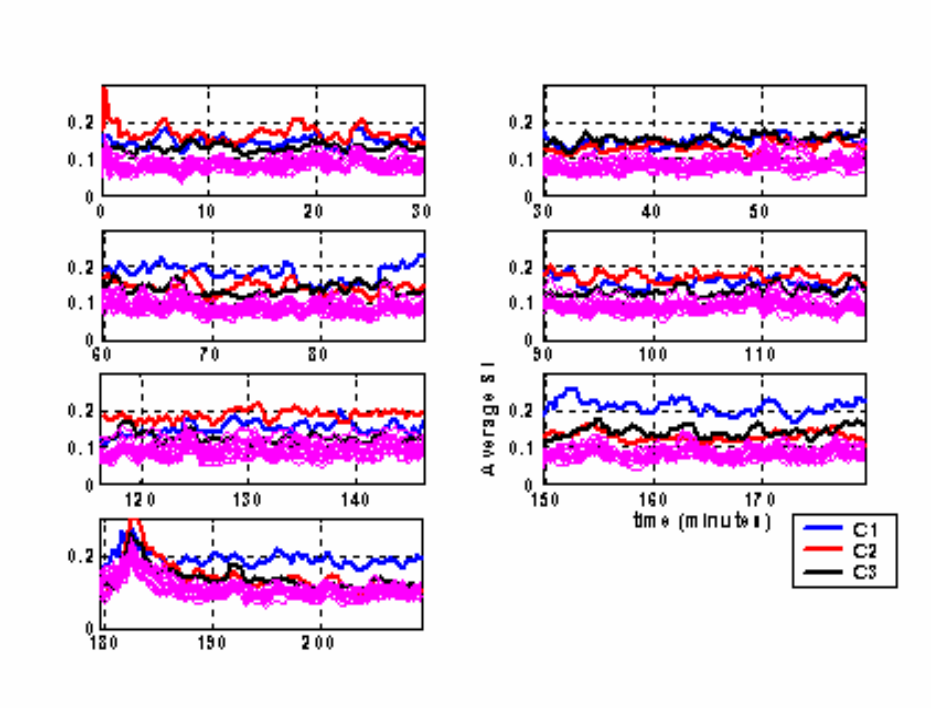

Figure 7. Statistical validation of the clustering results in patient P093. In each panel, thick lines are used to represent the profiles of the three clusters in a 30 minute time interval. The thin lines are the surrogate profiles indicating between-cluster interactions. Cluster veracity can be visually verified by observing that amplitudes representing within-cluster interaction for cluster profiles are mostly higher that the amplitudes representing between-cluster interaction for surrogate profiles, at each time-instance.

Seizures 4, 5, 6 & 7:

Spatio-temporal clustering analyses, similar to the one described on seizure 11 were performed on several other seizures, of the same patient P093. The cluster-similarity matrices ***P*** obtained from time-intervals surrounding seizures 4 & 5 and 6 & 7 of patient P093 are shown in fig 8. & fig 9. respectively. Channel groupings for the same are listed in tables 5 & 6, respectively All the 4 seizures present very consistent groupings.

1. Consistent to the observation in seizure 11, we observe the temporal depth and the sub-cortical regions of the left hemisphere are always bunched together.

2. Once again, the association of ROF-LOF areas into same cluster suggests a strong homologous connection between the orbito-frontal areas of the brain. This observation is also in agreement with those in seizure 11.

3. The dendrograms once again presented 4 unambiguous clusters in the form of RST, RTD, LST/LTD and LOF/ROF. The fusion levels, indicating the strength of connection between

clusters, often turn out in favor of RTD and RST to be grouped separately. Owing to the fact that we have pre-defined the number of clusters to 3, the LST, LTD, LOF & ROF channels will consequently get grouped into one cluster.

4. Once again, temporal changes are not very evident in the spatial patterns. However, observing fig 8 & fig 9 and their corresponding dendrograms (not shown), the fusion levels and the topology of the connections change with time. These changes can only be quantified using statistical tests such as Mantel test statistics or the Double Permutation Statistics (DPS).

Table 5. Spatio-temporal groupings as obtained for seizures 4 and 5 of patient P093.

P093, Seizure 4 & 5	**C_1**	**C_2**	**C_3**
Pre seizure 4, (30 – 60 mins)	RTD, RST	LOF, ROF	LTD, LST
Pre seizure 4, (0 – 30 mins)	RTD, RST	LOF, ROF	LTD, LST
Post seizure 4, (0 – 30 mins)	RTD	LTD, LST, LOF, ROF	RST
Post seizure 4, (30 mins – 1 hr)	RTD	LOF, ROF	LTD, LST, RST
Pre seizure 5, (30mins – 1 hr)	RTD	LTD, LST, LOF, ROF	RST
Pre seizure 5, (0 - 30mins)	RTD	LTD, LST, LOF, ROF	RST
Post-Seizure 5, (30 – 1 hr)	RTD	LTD, LST, LOF, ROF	RST

Table 6. Spatio-temporal groupings as obtained for seizure 6 and 7 of patient P093.

P093, Seizure 6 & 7	**C_1**	**C_2**	**C_3**
Post seizure 6, (0 - 30 mins)	RTD, RST	LTD, LST	LOF, ROF
Pre seizure 7, (30 mins – 1 hr)	RTD, RST	LTD, LST	LOF, ROF
Pre seizure 7, (0 – 30 mins)	RTD	LTD, LST, LOF, ROF	RST
Post seizure 7, (0 – 30 mins)	RTD	LTD, LST, RST	LOF, ROF
Post seizure 7, (30mins – 1 hr)	RTD	LTD, LST, LOF, ROF	RST

Post seizure 7, (1 hr – 1.5 hrs)	RTD	LTD, LST, LOF, ROF	RST

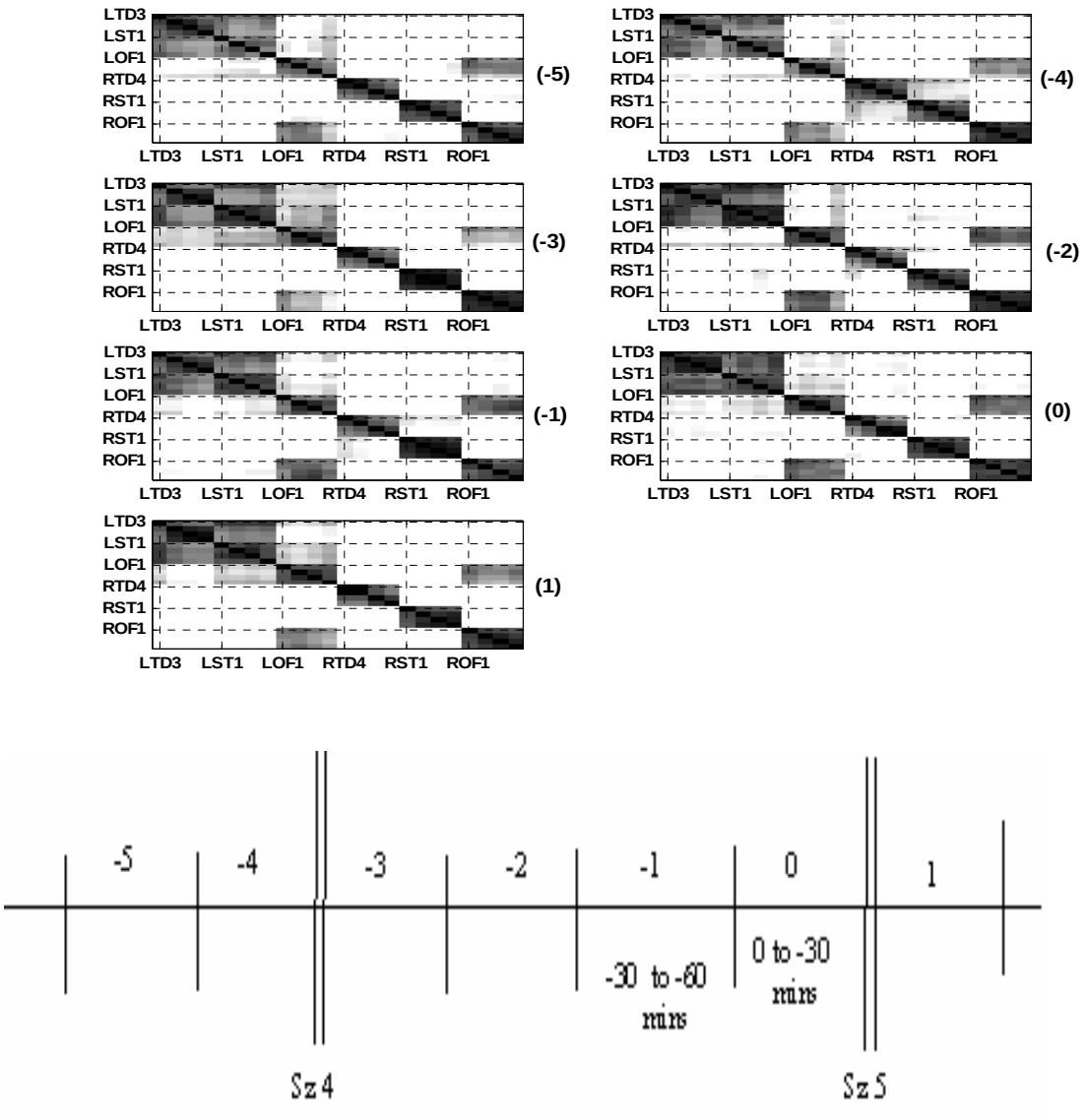

Figure 8. Seizures 4 and 5 of patient P093: Cluster-similarity matrices indicating the probability that two channels share the same cluster label in a 30 minute time-interval.

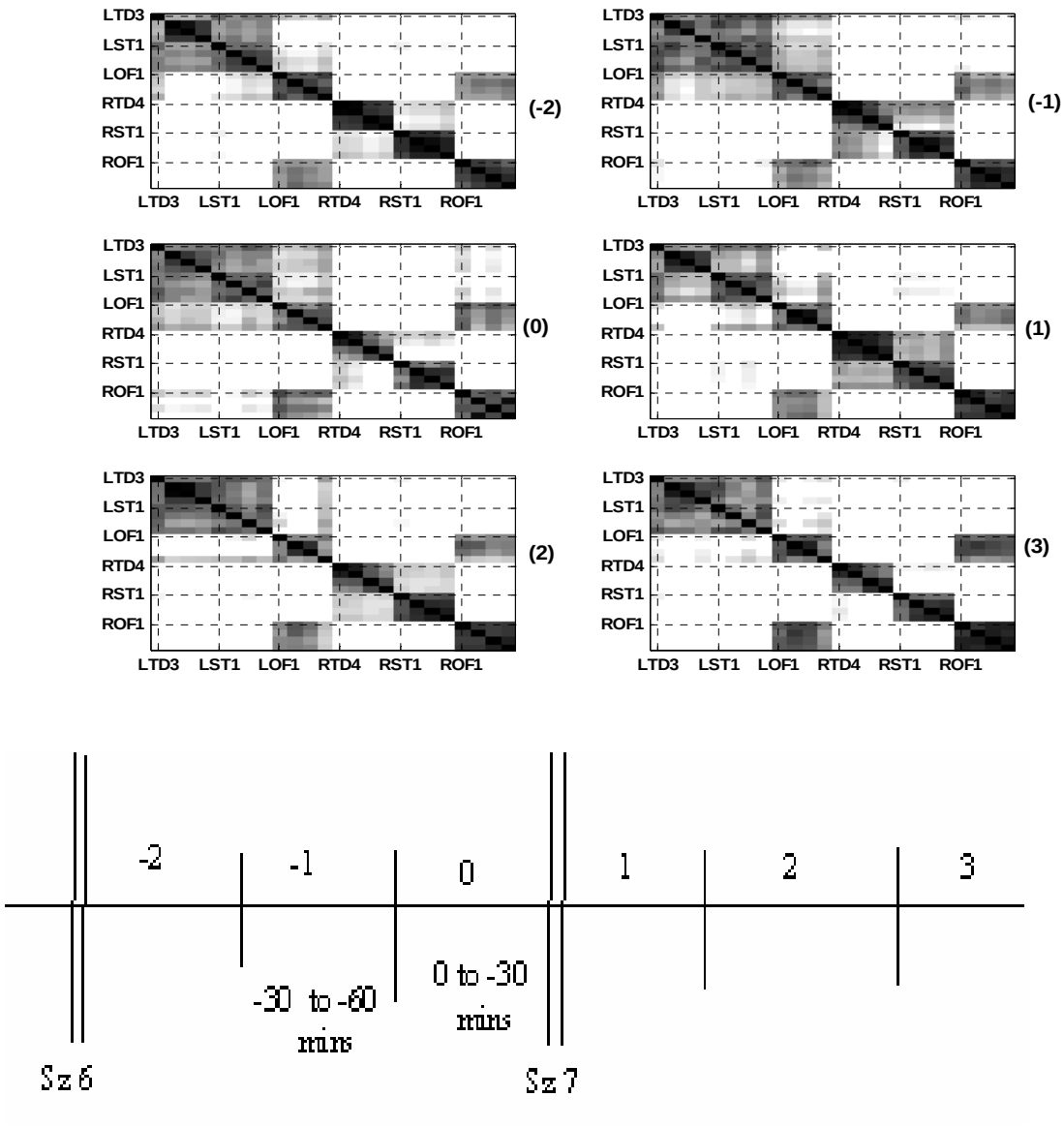

Figure 9. Seizures 6 and 7 of patient P093: Cluster-similarity matrices indicating the probability that two channels share the same cluster label in a 30 minute time-interval.

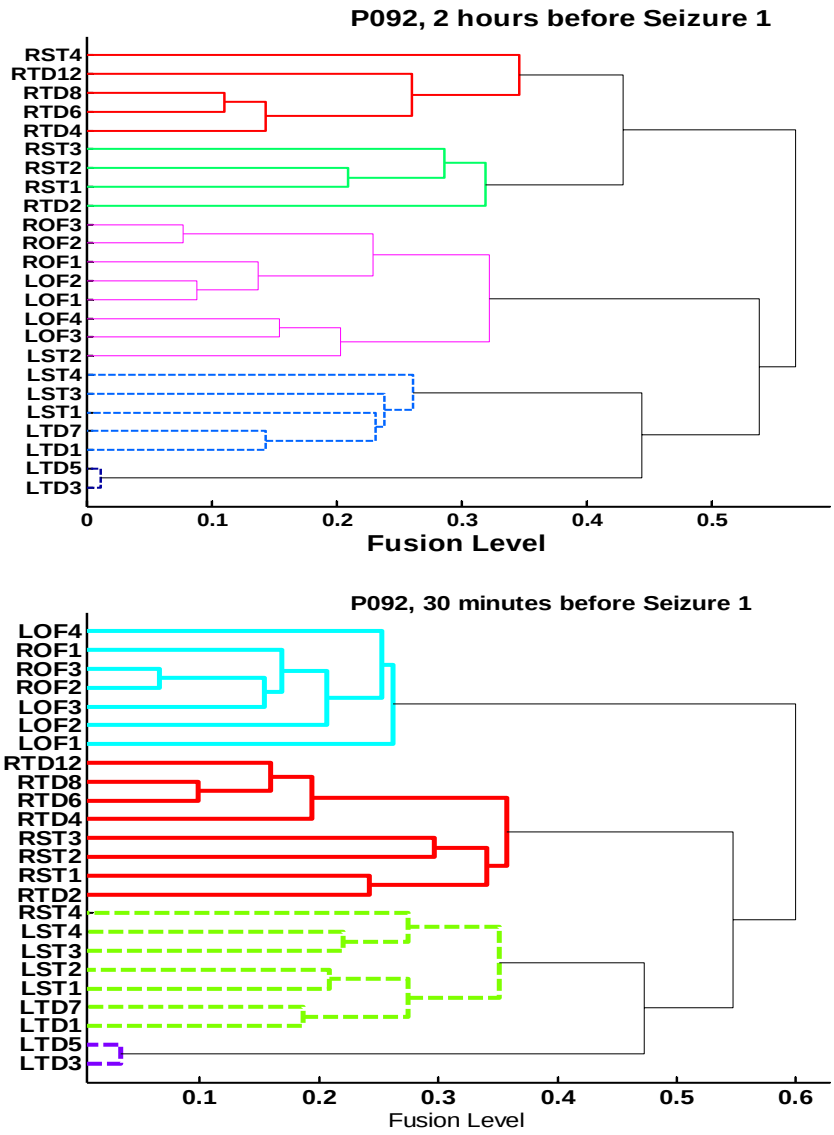

Figure 10. Dendrograms corresponding to P092, Seizure 1. Top: 2 hours before Seizure Bottom: 30 minutes pre-seizure.

Patient P092

In this section, we present the summary results of the clustering analyses performed on patient P092 suffering from a lesion in the medial temporal lobe structures of the right hemisphere.

Channel configuration for the patient P092 is as follows:

Channels 1 to 4: {LTD1, LTD3, LTD5, LTD7}

Channels 5 to 9: {RTD2, RTD4, RTD6, RTD8, RTD12}

Channels 10 to 13: {LST1, LST2, LST3, LST4}

Channels 14 to 17: {RST1, RST2, RST3, RST4}

Channels 18 to 21: {LOF1, LOF2, LOF3, LOF4}

Channels 22 to 24: {ROF1, ROF2, ROF3}

Note that a separate 2 dimensional 25x25 sized EEG-SOM grid was created to model the data dynamics of P092. Post spectral clustering analysis on 30 minutes data segments led to some interesting observations.

Fig 10. shows the dendrograms created for seizure segments 2 hours prior to seizure 1 and 30 minutes pre-seizure, respectively. As before, the number of clusters (n_1) specified in the spectral-clustering step after SOM-SI block was fixed to 3. The fusion levels between most of the channel clusters is greater than 0.4, indicating a lack of strong connectivity between regions.

For the second level of clustering, as before, let the number of clusters n_2 be fixed at 3. Cluster analysis on the 30 minutes segment 2 hours prior to seizure 1 (top dendrogram in Fig. 10) results in the following groups of channels:

Cluster #1: LTD & LST

Cluster #2: RTD & RST

Cluster #3: LOF & ROF

Observe the cluster formed from LTD & LST channels, in the dendrogram. It is made up of two sub-clusters, a large and a small cluster. The small cluster consists of only two channels, LTD (3 & 5) and fuses with the other sub-cluster at a very high fusion level (implying weak link). If n_2 was to be increased to 4, the clustering algorithm would classify this sub-cluster as an independent cluster. A detailed analysis on all seizures in P092 revealed a strong intra-channel correlation (or low fusion level) between channels LTD (3 & 5) and a weak inter-channel correlation with the rest of the channels. Surrogate analysis also confirmed the imbalance by having very few rejections for the cluster consisting of LTD (3 & 5) channels. It is obvious that the average interaction (within-cluster interaction) of the largest cluster would be pulled down if there are sub-clusters that have a strong within-sub-cluster interaction, but a weak between-sub-cluster interaction. Consequently, the within-cluster interaction of the largest cluster can be expected to be as weak as or marginally better than the between-cluster interactions, leading to fewer rejections of the null hypothesis H_0.

This problem can possibly be overcome by increasing the number of clusters to 4 or more. However, for consistency, we let the number of clusters n_2 be fixed at 3 in the rest of the analyses.

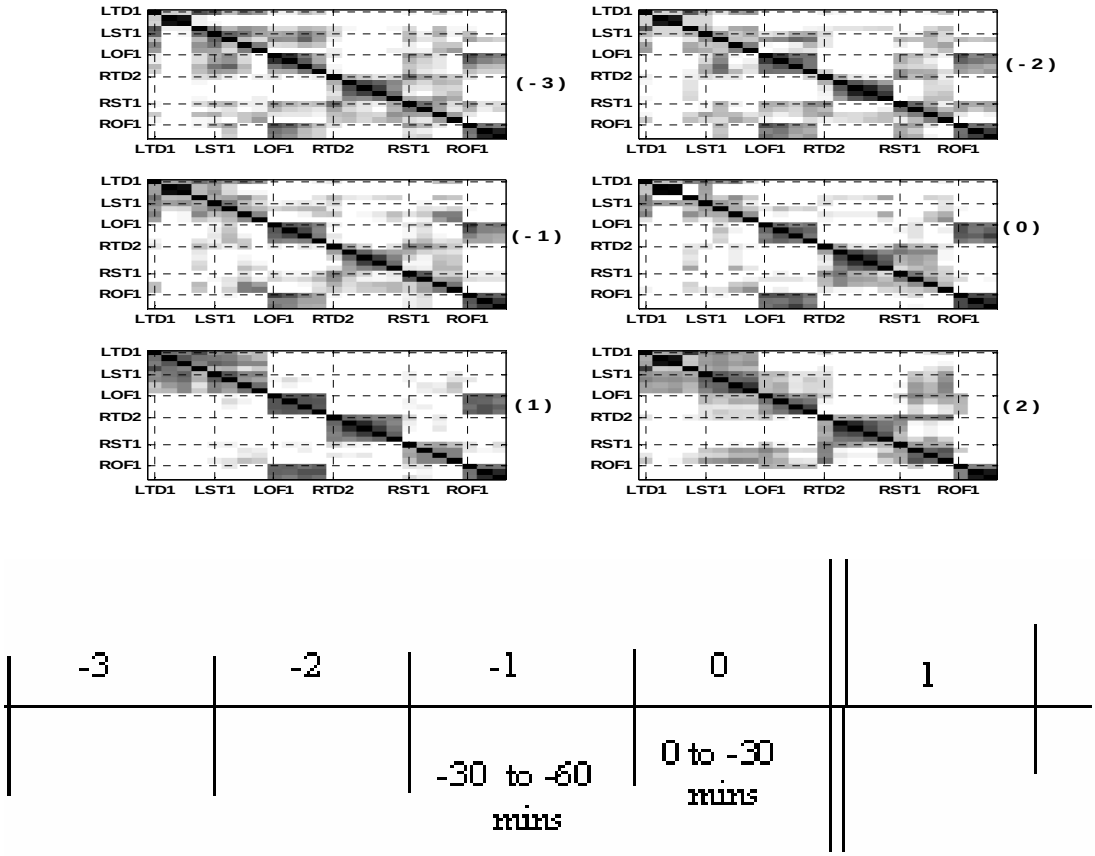

Figure 11. Cluster-similarity matrices indicating the probability that two channels share the same cluster label in a 30 minute time-interval. Top) Seizure 1 of patient P092

Seizures 1, 3 & 4:

For illustration, the cluster-similarity matrices corresponding to seizure 1 is shown in fig.10. Overall, the spatio-temporal clustering results for seizures 1, 3 & 4 are summarized in tables 7 to 9.

Table 7. Spatio-Temporal groupings as obtained for seizure 1 of Patient P092.

P092, Seizure 1	**C_1**	**C_2**	**C_3**
Pre seizure, (1.5 – 2 hrs)	RTD, RST	LTD, LST (1,3,4)	LOF, ROF, LST (2)
Pre seizure, (1 – 1.5 hrs)	RTD	LST, RST, LOF, ROF, LTD (1,7)	LTD (3,5)
Pre seizure, (30 mins – 1 hr)	RTD, RST	LTD, LST	LOF, ROF
Pre seizure, (0 - 30 mins)	RTD, RST	LTD, LST	LOF, ROF
Post-Seizure, (0 – 30 mins)	RTD, RST	LTD, LST	LOF, ROF

Post-Seizure, (30 – 1 hr)	RTD	LTD, LST, LOF, RST	ROF

Table 8. Spatio-Temporal groupings as obtained for seizure 3 of Patient P092.

P092, Seizure 3	**C_1**	**C_2**	**C_3**
Pre seizure, (1.5 – 2 hrs)	RTD	LST, LTD, RST	LOF, ROF
Pre seizure, (1 – 1.5 hrs)	RTD	LST, LTD, RST	LOF, ROF
Pre seizure, (30mins – 1 hr)	RTD, RST	LST, LTD	LOF, ROF
Pre seizure, (0 - 30mins)	RTD, RST	LST, LTD	LOF, ROF
Post-Seizure, (0 – 30 mins)	RTD, RST	LST, LTD	LOF, ROF
Post-Seizure, (30 – 1 hr)	RTD, RST	LST, LTD	LOF, ROF

Table 9. Spatio-Temporal groupings as obtained for seizure 4 of Patient P092.

P092, Seizure 4	**C_1**	**C_2**	**C_3**
Pre seizure, (1.5 – 2 hrs)	RTD, RST	LST, LTD	LOF, ROF
Pre seizure, (1 – 1.5 hrs)	RTD, RST	LST, LTD	LOF, ROF
Pre seizure, (30mins – 1 hr)	RTD	LST, LTD, RST	LOF, ROF
Pre seizure, (0 - 30mins)	RTD, RST	LST, LTD	LOF, ROF
Post-Seizure, (0 – 30 mins)	RTD, RST	LST, LTD	LOF, ROF
Post-Seizure, (30 – 1 hr)	RTD, RST	LST, LTD	LOF, ROF

From the cluster results of patient P092, we note the following:

1. The non-focal zone LTD has a strong coupling with the LST region. Correspondingly, strong affinity is observed between RTD and RST as well. These observations are consistent with the observations for P093. However, unlike in P093, we also see here that LTD connects and disconnects with several other channels, depending on the seizure state.

2. As in P093, we observe an exclusively strong connection between ROF-LOF regions at all stages surrounding a seizure. There are few instances where the ROF breaks into a separate group. We do not have any explanation for this drift in ROF, at this point in time.

3. Statistics from the surrogate analyses confirmed the veracity of the technique in most of the cases. As pointed out earlier, discrepancies occurred in a few instances for the clusters containing LTD (3, 5) channels.

Finally, we summarize the analysis on 2 patients and 8 complex partial seizures:

1. Contrary to the stand point that the seizure activity initiates in the focal zone followed by a gradual propagation to other regions, we observed that the spatial organization reflected by EEG activity exhibits either minimum or no progressive changes from the focal zone (RTD) to other zones (based on how it groups with other regions in the brain).

2. Evidence show stronger ipsilateral connection between the LTD and LST zones compared to the connection strength between RTD-RST. Statistical analysis to check if a significant difference in intra-hemisphere coupling strengths exists is needed.

3. We also found evidence to show a strong cross-hemispheric activity by observing consistent groupings of the right and left orbito-frontal lobes at all seizure states.

4. On how the overall spatial networks change every 30 minutes, patient P093 was seen to have qualitatively, lesser spatio-temporal changes in its ***P*** matrices than P092. It remains to be checked whether a significant change in the spatial organization before seizure is a pre-requisite to its subsequent occurrence. .

6. Discussion

In this study, we applied the SOM-based similarity index measure to analyze the mutual interactions among critical areas of an epileptic brain. Based on the functional relationships, we analyzed long term structural connectivity's related to various seizure states by proposing a spatio-temporal clustering model. On analyzing 8 complex partial seizures from 2 patients suffering from temporal lobe epilepsy, we found that the orbito-frontal regions always exhibit a strong homologous connectivity while maintaining a low relationship with other regions. The left sub-temporal and the left-temporal depth regions (non-focal hemisphere) were identified to have a strong ipsilateral connection, regardless of seizure states. Finally, we found that the epileptic zone, namely the right hippocampus depth region maintained a relatively strong connection with the right sub-temporal region. Interestingly, the configuration of the groupings between different regions always remained the same, regardless of whether the patient was in an inter-ictal, pre-ictal or post-ictal state although the inter-region connectivity strengths seemed to vary slightly across states.

So far, because of the data size, we were constrained to analyze only on 8 seizures from 2 patients. Future effort in this direction would be to apply the proposed approach on a larger set of seizures and more patients. In addition, since we analyzed only on complex partial seizures, it would be worthwhile to check the cluster grouping in other types of seizures such as partial secondary generalized and sub-clinical seizures.

Recall from the results that certain channels were always grouped together regardless of the seizure states. This raises a question if this pattern is unique to an epileptic patient and therefore be considered as a blueprint of seizures. One plausible way to answer this speculation would be to apply the proposed clustering approach on normal subjects and then compare the differences in groupings with that of seizure patients

One of our other main objectives in this study was to develop engineering tools to determine spatio-temporal groupings in a multivariate epileptic brain. We proposed a similarity-based clustering approach and used it to extract hidden structures from an epileptic brain. One of the obvious limitations with any clustering approach is determining the optimal number of clusters. Techniques to combat the cluster size problems have been researched upon, without much success. In eigen vector based methods such as spectral clustering, cluster size can possibly be approximated to be equal to the number of eigen vectors corresponding to significant eigen values. In multiple data sets however, the optimal cluster size need not have to be the same across different data sets rendering cluster comparisons weak. In our approach, we analyzed a large number of data sets and empirically, fixed the cluster size to 3. This may not be an efficient or a systematic approach to tackle the problem. Theoretic efforts are needed to develop mathematical criterion that allows us to determine a fixed cluster size, suitable to all groups of data. Besides, exploring tools better than clustering to unravel hidden patterns in multidimensional time-sequences would be very beneficial.

REFERENCES

[1] L. D. Iasemidis, J. C. Principe, J. M. Czaplewski, R. L. Gilmore, S. N. Roper, and J. C. Sackellares, *Spatiotemporal Transition to Epileptic Seizures: a Nonlinear Dynamical Analysis of Scalp and Intracranial EEG Recordings*. In: Lopes da Silva F. H., Principe J. C., Almeida L. B., eds. S*patiotemporal models in biological and artificial systems.* Amsterdam: IOS Press, pp: 81-89, 1997

[2] L. D. Iasemidis, L. D. Olson, J. C. Sackellares, and R. Savit, “Time Dependencies in the Occurrence of Epileptic Seizures: a NonLinear Approach,” *Epilepsy Research*, vol. 17, pp. 81-94, 1994.

[3] K. Blinowska, R. Kus, and M. Kaminski, “Granger Causality and Information flow in Multivariate processes,” *Physical Review E*, vol. 70: 050902, pp: 01-04, 2004.

[4] J. Arnhold, P. Grassberger, K. Lehnertz, and C. E. Elger, “A Robust Method for Detecting Interdependencies: Application to Intracranially Recorded EEG,” *Physica D*, vol. 134, pp. 419-430, 1999.

[5] A. Hegde, D. Erdogmus, Y. Rao, J. C.Principe, and J. B.Gao, “SOM-Based Similarity Index Measure: Quantifying Interactions Between Multivariate Structures,” *Proceedings of NNSP’03, pp. 819-828, Toulouse, France*, Sep 2003.

[6] A. Hegde, D. Erdogmus and J. C. Principe, “Synchronization Analysis of Epileptic ECoG Data Using SOM-Based SI Measure,” *Proceedings of EMBS 2004*, pp. 952-955, San Francisco, September 2004.

[7] S. Haykin, *Neural Networks: A Comprehensive Foundation*, 2nd edition, Prentice Hall, 1999.

[8] J. C. Principe, N. R. Euliano, and W. C. Lefebvre, *Neural and Adaptive Systems: Fundamentals through Simulations*, John Wiley & Sons, 2000.

[9] A. Hegde, D. Erdogmus, and J. C. Principe, “Quantifying Spatio-Temporal Dependencies in Epileptic ECOG,” *IEEE Signal Processing Special Issue - 'Neural Co-ordination in the Brain*; A Signal Processing Perspective', vol. 85, pp. 2082-2100, 2005.

[10] J. A. Garcia, J. Fdez-Valdivia, F. J. Cortijo, and R. Molina, “A Dynamic Approach for Clustering Data,” *Signal Processing*, vol. 44(2), pp. 181-196, 1995.

[11] E. Keogh, J. Lin, and W. Truppel, “Clustering of Time Series Subsequences is Meaningless: Implications for Past and Future Research” *Proceedings of the 3rd IEEE International Conference on Data Mining* (ICDM 2003), pp.115-122, Melbourne, Florida, 2003.

[12] A. Y. Ng, M. I. Jordan, and Y. Weiss, “On Spectral Clustering: Analysis and an Algorithm,” *Advances in Neural Information Processing Systems*, 14, pp. 849-856, 2002

[13] J. Malik, S. Belongie, T. Leung, and J. Shi, “Contour and Texture Analysis for Image Segmentation,” International Journal of Computer Vision, 43(1), pp. 7-27, 2001.

[14] L. D. Iasemidis, K. E. Pappas, J. C. Principe, and J. C. Sackellares, “SpatioTemporal Dynamics of Human Epileptic Seizures,” *Proceedings of the 3rd Experimental Chaos Conference*, eds. R.G. Harrison *et al.*, World Scientific, Singapore, pp. 26-30, 1996.

[15] L. D. Iasemidis, P. Pardalos, J. C. Sackellares, and D. S. Shiau, “Quadratic Binary Programming and Dynamical System Approach to Determine the Predictability of Epileptic Seizures,” *Journal of Combinatorial Optimization*, vol. 5, pp. 09-26, 2001.

[16] F. Takens, *Detecting Strange Attractors in Turbulence*. In: Rand DA, Young LS, eds. Dynamical systems and turbulence. Lecture notes on mathematics. vol. 898, Berlin: Springer, pp. 366-381, 1981.

[17] A. Hegde, D. Erdogmus, and J. C. Principe, "Spatio-Temporal Clustering in Epileptic ECOG," *Proceedings of EMBS,* Shanghai, September, 2005.

[18] D. Prichard, and J. Theiler, "Generating Surrogate Data for Time Series with Several Simultaneously Measured Variables," *Physical Review Letters*, vol. 73 (7), pp. 951-954, 1994

[19] T. Schreiber, "Measuring Information Transfer," *Physics Review Letters*, vol. 85, pp. 461-470, 2000.

[20] T. Schreiber, and A. Schmitz, "Improved Surrogate Data for Nonlinearity Tests," *Physical Review Letters*, vol.77 (4), pp. 635-638, 1996.